Itinerant nature of U 5*f* states in uranium mononitride revealed by angle-resolved photoelectron spectroscopy

Shin-ichi Fujimori,[1,*] Takuo Ohkochi,[1,†] Tetsuo Okane,[1] Yuji Saitoh,[1] Atsushi Fujimori,[1,2] Hiroshi Yamagami,[1,3] Yoshinori Haga,[4] Etsuji Yamamoto,[4] and Yoshichika Ōnuki[4,5]

[1]*Condensed Matter Science Division, Japan Atomic Energy Agency, Sayo, Hyogo 679-5148, Japan*
[2]*Department of Physics, University of Tokyo, Hongo, Tokyo 113-0033, Japan*
[3]*Department of Physics, Faculty of Science, Kyoto Sangyo University, Kyoto 603-8555, Japan*
[4]*Advanced Science Research Center, Japan Atomic Energy Agency, Tokai, Ibaraki 319-1195, Japan*
[5]*Graduate School of Science, Osaka University, Toyonaka, Osaka 560-0043, Japan*

(Received 27 July 2012; published 6 December 2012)

The electronic structure of the antiferromagnet uranium nitride (UN) has been studied by angle-resolved photoelectron spectroscopy (ARPES) using soft x-rays ($h\nu = 420$–520 eV). Strongly dispersive bands with large contributions from the U 5*f* states were observed in ARPES spectra and form Fermi surfaces. The band structure as well as the Fermi surfaces in the paramagnetic phase are well explained by the band-structure calculation treating all the U 5*f* electrons as being itinerant, suggesting that an itinerant description of the U 5*f* states is appropriate for this compound. On the other hand, changes in the spectral function due to the antiferromagnetic transition were very small. The shapes of the Fermi surfaces in a paramagnetic phase are highly three-dimensional, and the nesting of Fermi surfaces is unlikely as the origin of the magnetic ordering.

DOI: 10.1103/PhysRevB.86.235108 PACS number(s): 79.60.−i, 71.27.+a

I. INTRODUCTION

The origin of magnetism has been one of the controversial issues in *f*-electron materials. Generally, in rare-earth 4*f* compounds, a long-range magnetic ordering is understood by the Ruderman-Kittel-Kasuya-Yoshida interaction, which is essentially based on a localized *f*-electron picture. On the other hand, the origin of magnetism in actinide 5*f* compounds has been not well understood since the 5*f* electrons show magnetic properties of both itinerant and localized properties. Although there are a number of studies on the magnetism of actinide-based compounds, there are only a few cases where the origin of magnetism has been directly revealed.[1,2]

In the present study, we report an angle-resolved photoelectron spectroscopy (ARPES) study on uranium mononitride (UN) to understand its electronic structure as well as to explore the origin of magnetism in 5*f* compounds. UN has a NaCl-type face center cubic (fcc) crystal structure in the paramagnetic (PM) phase, and it undergoes a transition into the type I antiferromagnetic (AFM) phase with $T_N = 53$ K and $\mu_{ord} = 0.75\ \mu_B$. Although a band antiferromagnetism has been suggested for UN,[3] there are still controversial issues regarding the magnetic and electronic properties.

Samsel-Czekała *et al.* have studied the magnetic and transport properties of UN.[4] They have discussed their data based on the dual and spin-density-wave picture of the U 5*f* states, but a definitive conclusion was not reached. Solontsov and Silin[5] suggested that UN is a weak itinerant-electron antiferromagnet which has a different mechanism from the nesting of the Fermi surface. They have suggested that the magnetic ordering is caused by the polarization of bands rather than the spin-density-wave-type Fermi surface instability. Therefore, it is essential to reveal the overall electronic structure of UN to understand the nature of U 5*f* states in UN.

The electronic properties of UN have been studied experimentally[4,6–9] and theoretically.[10,11] Reihl *et al.* first measured ARPES spectra of UN by using an incident photon energy of $h\nu = 25$ eV with the energy resolution of $\Delta E = 150$ meV.[6] They observed the temperature dependence of the spectra and suggested the itinerant nature of U 5*f* states. However, they measured the normal emission spectrum only, and the overall electronic structures of U 5*f* states were not well understood. Subsequently, Itoh *et al.* performed higher energy resolution ARPES experiments on UN by using $h\nu = 21.2$ eV with $\Delta E = 50$ meV and observed two-dimensional energy band dispersions. They observed two nondispersive U 5*f* bands in addition to dispersive N *s* and *p* bands.[7] One is located just below E_F, and the other is located at $E_B = 0.6$ eV. Therefore, they suggested that U 5*f* electrons have dual (itinerant and localized) natures. Meanwhile, a recent x-ray photoelectron spectroscopy study on UN showed that the U 4*f* core-level spectrum shows an asymmetric line shape characteristic of a metal and multiple final-state structures, which were also interpreted as the dual nature of U 5*f* states. From the theoretical point of view, it has been suggested that the electronic structure cannot be understood within the framework of a local density approximation (LDA). Modak and Verma[10] studied the electronic structure of UN by the LDA, as well as the generalized-gradient approximation, and suggested that the LDA is insufficient for the description of its electronic structure. Moreover, Yin *et al.*[11] theoretically calculated the thermal conductivity of actinide nitrides by means of the dynamical mean-field theory and pointed out that the electron correlation effect (the Hubbard *U*) is essential to describe its electrical properties. Therefore, an appropriate theoretical framework for its description is still not known.

In addition to this scientific interest, there is a practical demand to study UN's electronic structure. UN is a promising fuel material for the generation IV advanced nuclear reactors since it has a high melting point (2850 °C), a very good thermal conductivity at high temperatures, and a high fuel density (14.32 g cm^{-2}).[12] It is quite important to clarify its

electronic structure to design better fuel materials.[11] Moreover, understanding it is essential to comprehending the reaction of UN with water or oxygen for the safety of nuclear power plants as well as for the storage of fuel materials.[13]

II. EXPERIMENTAL PROCEDURE

Photoemission experiments were performed at the soft x-ray beamline BL23SU of SPring-8.[14] The overall energy resolution in the angle-integrated photoemission (AIPES) experiments at $h\nu = 800$ eV was about 110 meV, and that in the ARPES experiments at $h\nu = 420$–520 eV was 80–120 meV, depending on the experimental setup. The position of the Fermi level (E_F) was carefully determined by measurements of the evaporated gold film. Clean sample surfaces were obtained by *in situ* cleaving the sample with the surface parallel to the (001) plane. The positions of ARPES cuts were calculated by assuming free-electron final states with an inner potential of $V_0 = 12$ eV.

III. RESULTS AND DISCUSSION

A. Angle-integrated photoemission spectra

First, we present the angle-integrated photoemission spectra of UN. Figure 1(a) shows the valence-band spectrum of UN taken at $h\nu = 800$ eV. The sample temperature was 75 K, and the compound is in the PM phase. In this photon energy range, the contribution from the U $5f$ states is dominant, and those from the N s and p states are two or three orders of magnitude smaller than that of the U $5f$ states.[15] In the valence-band spectrum, there is a sharp peak structure just below E_F. This peak structure has a strong contribution from the U $5f$ states. On the other hand, weak and broad peak structures distributed at 2–6 eV are ascribed to contributions from the N s and p states. For comparison with the experimental data, we have performed band-structure calculations treating all U $5f$ electrons as being itinerant. The calculation is a relativistic-linear augmented-plane-wave band-structure calculation[16] within the LDA.[17] In Fig. 1(a), the calculated U $5f$ partial density of states broadened with the instrumental resolution is also indicated. It has an asymmetric line shape, with a long tail towards higher binding energies. The overall spectral line shape is consistent with the calculation.

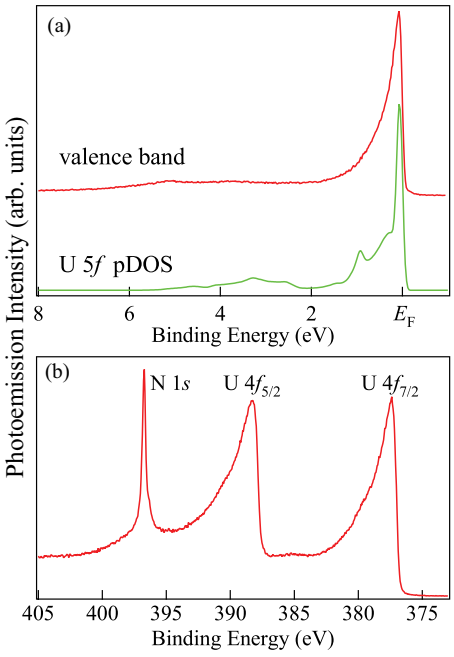

FIG. 1. (Color online) Angle-integrated photoemission spectra of UN measured with $h\nu = 800$ eV. (a) Valence-band spectrum with the calculated U $5f$ partial density of states broadened by the instrumental resolution. (b) U $4f$ core-level spectrum.

Figure 1(b) shows the U $4f$ core-level spectrum of UN taken at $h\nu = 800$ eV. It shows a spin-orbit splitting corresponding to U $4f_{7/2}$ and U $4f_{5/2}$, and both of them have a broad asymmetric line shape. This is a common feature of U $4f$ core-level spectra of metallic uranium compounds. The spectrum shows a relatively simple main line shape with large asymmetry.[18] This spectral line shape is similar to that of itinerant U $5f$ compounds. The binding energy of the U $4f_{7/2}$ main line is 377.27 eV, which is in good agreement with the previous study on UN thin film (377.3 eV).[8,19] This is within the binding energies of the $5f^4$ final-state peak of various itinerant uranium compounds,[18] suggesting that UN can be classified into itinerant uranium compounds. In the previous photoemission experiment, a small satellite structure was observed at a higher binding energy side by 3 eV than that of the main line.[4] The authors have argued that this satellite originates from different valence states and suggested this is an indication of the dual nature of U $5f$ states in this compound. However, there is no such satellite structure in the present U $4f$ spectrum. Since the peak position of the small satellite corresponds to that of UO_2, this satellite may originate from an oxidized component of their sample surfaces.

B. Band structures

Figure 2(a) shows the ARPES spectra of UN measured along the X-W-X line. The sample temperature was kept at 75 K in the PM phase. The position of the ARPES cut in momentum space was calculated based on the free electron final sates, and the photon energy used was 490 eV. The experimental energy resolution was 85 meV. In the ARPES spectra, clear energy dispersions were observed. In the vicinity of E_F, there exists a highly dispersive band with a strong intensity. This band has a large contribution from the U $5f$ states, especially in the vicinity of E_F. As the band goes from the W point to the X point in the first Brillouin zone, it approaches E_F. Near the midpoint of the X-W line, its intensity suddenly decreases, suggesting that it crosses E_F. Meanwhile, weak but finite photoemission intensities, just below E_F, persist outside the Fermi momentum (k_F). A similar phenomenon has been observed in the ARPES spectra of other uranium compounds.[20] Its origin is discussed below. On the high-binding-energy side ($E_B = 1.5$–6 eV), there exist weak and strongly dispersive bands. Since they have intensities weaker than those of bands near E_F, they are assigned to contributions mainly from the N s and p bands. The overall structure of the present spectra are very similar to the previous results measured by He I ($h\nu = 21.2$ eV)[7], but there is one striking difference between them. In the previous ARPES study, two nondispersive bands

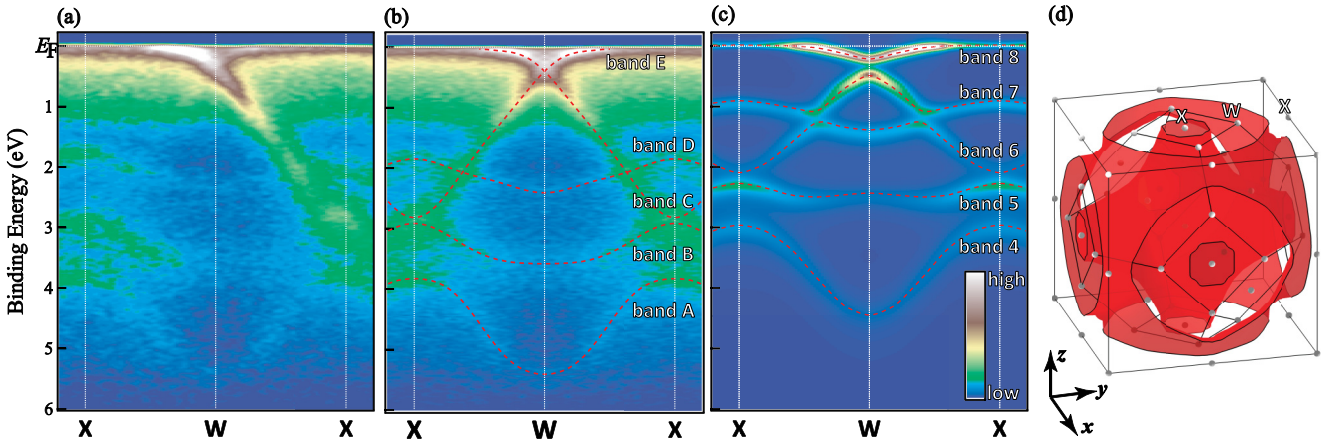

FIG. 2. (Color online) ARPES spectra and comparison with the results of band-structure calculations. (a) ARPES spectra measured along the X-W-X line. (b) Symmetrized ARPES spectra. Dashed curves are guides for the eye. (c) Simulation of ARPES spectra based on the band-structure calculation treating all U 5f electrons as being itinerant. (d) fcc Brillouin zone of UN in the paramagnetic phase and calculated Fermi surfaces.

were observed in the vicinity of E_F.[7] One is located just below E_F, while the other is located around $E_B \sim 0.6$ eV, and they were assigned to the itinerant and localized components, respectively. This has been considered an indication of the dual nature of the U 5f electrons in UN. However, we have observed a single itinerant band in the vicinity of E_F, and the dual nature of the U 5f electrons was not observed. These differences may originate from the higher surface sensitivity in the previous ARPES study.

Here, it should be noted that the intensities of the observed bands are not symmetric with respect to the W point. For example, the band located just below E_F has an asymmetric shape relative to the W point, and the intensity of its counterpart is very weak. Since their intensities depend on the Brillouin zone, this may be due to the photoemission structure factor (PSF) effect as has been observed in ARPES spectra of other materials.[21] To eliminate this effect, we have symmetrized the ARPES spectra relative to the W point as shown in Fig. 2(b). Dashed curves represent approximate positions of bands, estimated from the second derivatives of ARPES spectra. The band structure of UN is more easily understood from this image. There are five bands in this energy-momentum region, and they are called A, B, C, D, and E, from higher to lower binding energies. Band E forms an electron pocket around the W point, and it has a large contribution from the U 5f states. Bands A–D, on the high-binding-energy side, disperse strongly and are assigned to contributions mainly from the N s and p states.

To understand the validity of the itinerant description of the 5f states in this compound, we compare the present ARPES spectra with the result of the band-structure calculation within the LDA framework treating all the U 5f electrons as being itinerant. Figure 2(c) shows the band structure and a simulation of ARPES spectra based on the band-structure calculation, and Fig. 2(d) shows the fcc Brillouin zone of UN with the calculated Fermi surfaces. In this simulation, the following effects have been taken into account: (i) the broadening in the k_z direction due to the finite escape depth of photoelectrons, (ii) the lifetime broadening of the photohole, (iii) the photoemission cross sections of orbitals, and (iv) the energy resolution and angular resolution of the electron analyzer. The details are reported in the Appendix. Energy band dispersions corresponding to the X-W-X high-symmetry line are shown by dashed curves and are consistent with the results of the previous band-structure calculations.[22,23] In the band-structure calculation, band 8 forms the hole pocket Fermi surface around the W point. On the high-binding-energy side, there exist strongly dispersive bands with contributions mainly from the N s and p states. A comparison between ARPES spectra and the simulation shows that there is a good correspondence between the experimentally observed bands A–E and the calculated bands 4–8, respectively, though the binding energies of bands A–D are deeper in the experiment than in the calculation. On the other hand, there are some disagreements between the experiment and the calculation. For example, there is a clear gap structure between the bottom of band 8 and the top of band 7 in the band-structure calculation, while this is not clearly seen in the experiment. Bands 7 and 8 mainly consist of the N s and p states and the U 5f state, respectively, and the absence of a clear gap in the experimental spectra suggests that the hybridization between them is weaker in the experiment than in the calculation. Despite these discrepancies, the good one-to-one correspondence between them suggests that the band-structure calculation gives a reasonable description of the experimentally obtained band structure. Here, it should be noted that there exist finite photoemission intensities at E_F outside k_F in this simulation as was observed in the experiment. Their origin is mainly due to the finite broadening along momentum directions and the three-dimensionality of the electronic structure. Therefore, the finite intensities at the Fermi energy observed in the ARPES spectra of other uranium compounds such as UB_2 would be explained by this effect.

C. Temperature dependence of the band structure

Next, we show the changes in the electronic structure associated with the AFM transition. Before we show the

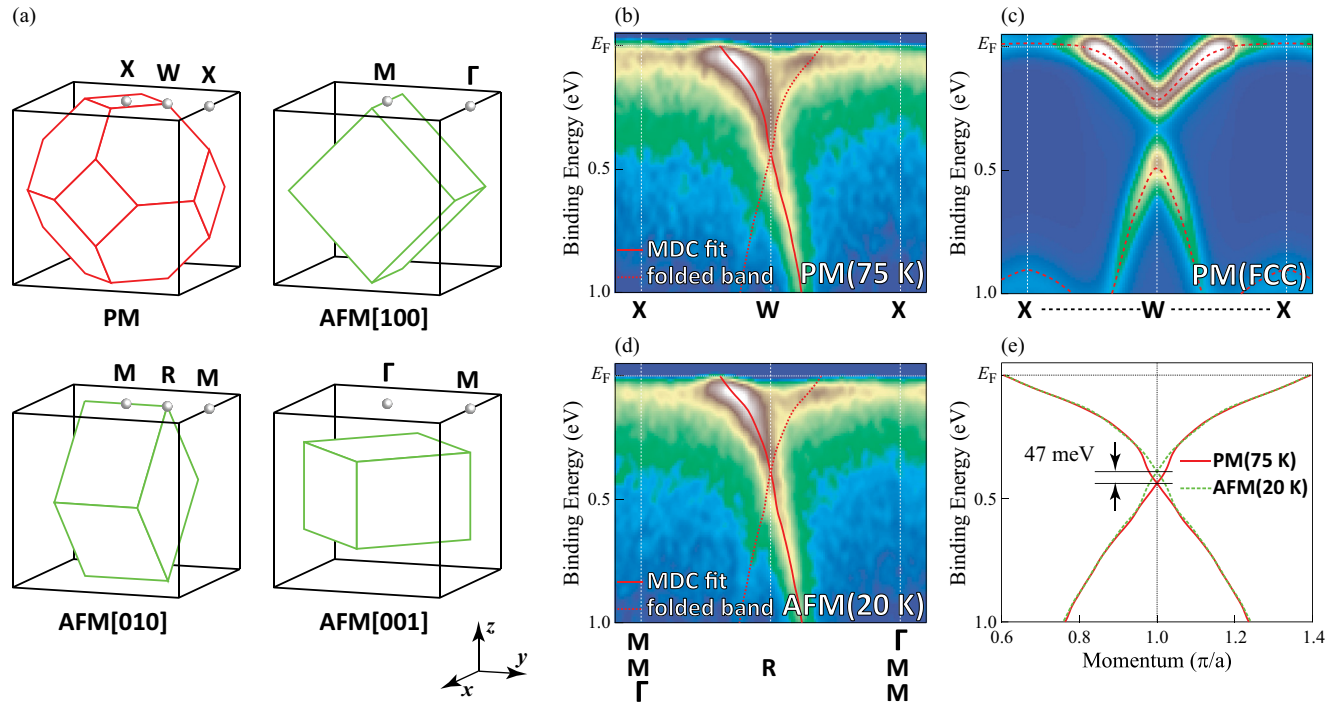

FIG. 3. (Color online) Temperature dependence of ARPES spectra. (a) Brillouin zone of UN in the PM phase and in the AFM phase with the AFM ordering wave vector along the [100], [010], and [001] directions. (b) ARPES spectra of UN in the PM phase measured along the X-W-X direction. (c) Simulation of ARPES spectra based on band-structure calculation of UN in the PM phase treating all the U 5*f* electrons as being itinerant. (d) ARPES spectra of UN in the AFM phase measured along the same direction as the scan in the PM phase. The scan corresponds to the M-Γ, M-R-M, and Γ-M directions in the AFM Brillouin zone. (e) Comparison of bands near E_F in the PM and AFM phases.

ARPES spectra, we explain the relationship between the ARPES scan in the PM phase and the AFM phase. In the PM phase, the crystal structure is fcc. In the AFM phase, the magnetic moments are aligned ferromagnetically within the (001) plane and are coupled antiferromagnetically between the neighboring (001) plane. There are three equivalent directions of the AFM ordering vector, [100], [010], and [001], and the Brillouin zone should be a diamond shape whose direction depends on the directions shown in Fig. 3(a). Since these ordering directions will form domains of a very small length, and the beam spot is expected to cover multiple domains, the ARPES spectra taken along the X-W-X direction in the PM Brillouin zone correspond to a mixture of signals from the M-Γ, M-R-M, and Γ-M directions in the AFM phase. The relationship between the PM and the AFM Brillouin zone is as shown in Fig. 3(a).

Figures 3(b) and 3(c) show blowups of the near-E_F region of ARPES spectra measured along the X-W-X direction and the calculated energy band dispersions in the PM phase. The positions of bands estimated from their momentum distribution curves (MDCs) and their folding are also shown in Fig. 3(b), by solid and dashed curves, respectively. The behavior of the quasiparticle band is more clearly recognized. Around the W point, there is a V-shaped band just below E_F, and it forms an electron pocket Fermi surface. Here, it should be noted that the fitted band has a larger slope than the calculated band in the vicinity of E_F. This seems to be inconsistent with the fact that the experimental band has an electron mass heavier than that of the band-structure calculation as inferred from the larger electronic specific heat coefficient in the experiment ($\gamma_e = 49$ mJ K^{-2}mol^{-1}) than in the calculation ($\gamma_e = 17.95$ mJ K^{-2}mol^{-1}). This might be due mainly to the very small energy scale of the renormalization of the experimental quasiparticle bands. In fact, the effect of the renormalization appears in the energy range of a few tens of meV in the vicinity of E_F in the quasiparticle bands of the heavy fermion compound USb_2.[24] If the quasiparticle band has a renormalization on a similar energy scale, the structure cannot be observed with the present experimental energy resolution. Moreover, a fitting of MDCs generally gives a slope larger than that of the actual band when the band is nearly flat and broad.[25] This can be inferred from Figs. 3(b) and 3(d), where fitting of the energy distribution curves should give nearly flat bands just below the E_F around k_F. Therefore, the peak positions estimated from MDCs in the vicinity of E_F do not correspond to the actual band positions in the present analysis.

Figure 3(d) shows the ARPES spectra measured by the same geometry as in Fig. 3(b) but at 20 K. The sample is in the AFM phase, and this scan direction would correspond to the M-Γ, M-R-M, and Γ-M directions in the AFM Brillouin zone. It is shown that the spectra do not show significant changes. Here we note that the N *s* and *p* derived bands located in the binding energy range $E_B = 1.5$–6 eV show no changes with the AFM transition. Back-folded replica bands due to the AFM Brillouin zone are not clearly observed. The MDC-fitted peak positions and their folding are shown by solid and dashed curves. The basic structure is essentially identical to those measured in the PM phase. Therefore, the changes in

ARPES spectra associated with the AFM transition are very small.

To see the changes in those bands in detail, we have compared the fitted bands in both phases. Figure 3(e) shows a comparison of the fitted bands between the PM and the AFM phases. Since these bands should be symmetric with respect to $k_x = \pi/a$, folded bands are also shown. The bands are almost identical in the PM and the AFM phases, buta small but clear difference exists around the zone boundary ($k_x \sim \pi/a$). As the compound undergoes the AFM phase transition, the crossing point of bands moves toward lower binding energies by about 47 meV. Since the electronic structure of this crossing point is affected by the folding of bands due to the magnetic ordering [010], this change is considered to be due to the PM-to-AFM transition. We consider the origin of this change in the discussion below.

D. Fermi surface

To reveal the overall shapes of the Fermi surfaces of UN in three dimensions, we have performed Fermi surface mapping by changing the photon energies. Figure 4(a) shows an intensity map of ARPES spectra obtained by changing the photon energy from 420 to 520 eV. The sample temperature was kept at 20 K, and the sample was in the AFM phase. Photoemission intensities within $E_F \pm 50$ meV of each ARPES spectra were integrated and mapped as a function of momenta parallel (k_y) and perpendicular (k_z) to the sample surface. A round-shaped Fermi surface around the X point is observed. Figures 4(b) and 4(c) show a simulation of Fermi surface mapping and the three-dimensional shape of the Fermi surface calculated by the band-structure calculation, respectively. Although the sample is in the AFM phase, the essential band structure near E_F does not show significant changes as shown in Fig. 3, and we have compared the experimental Fermi surfaces with the band-structure calculation in the PM phase. A large and round-shaped Fermi surface centered at the X point was observed, while a small and square-shaped Fermi surface centered at the X point was not clearly observed, although both of them originate from the same band. This is due to the PSF effect as observed in the ARPES spectra shown in Fig. 2(a). The cross sections of the Fermi surfaces are also shown by the solid (red) curves. Here, it should be noted that the photoemission intensities become strong outside and inside the round-shaped and square-shaped Fermi surfaces, respectively, in the simulation. This is due to the finite energy resolution (∼85 meV) as well as the finite energy window (∼100 meV) of the photoemission intensity integration, which make the image include intensities from bands below E_F. Although the size of the experimentally observed Fermi surface is slightly smaller than that of the calculation, the shape of the large round Fermi surface centered at the X point matches between experiment and calculation. Therefore, the experimental Fermi surfaces are well explained by the band-structure calculation. This result again suggests that an itinerant description is appropriate for the electronic structure of UN.

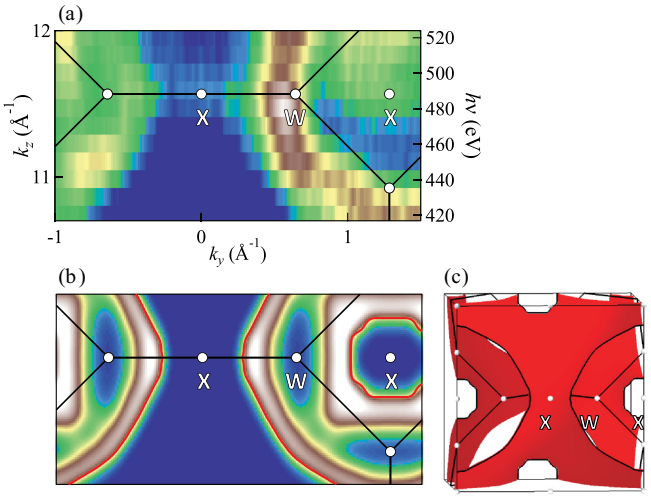

FIG. 4. (Color online) Fermi surfaces of UN. (a) Experimental Fermi surface mapping in the k_y-k_z plane obtained by changing the incident photon energy. (b) Simulation of Fermi surface mapping based on band-structure calculation treating all U 5f electrons as being itinerant. (c) Brillouin zone in the PM phase and calculated Fermi surfaces.

E. Discussion

As described above, we have observed the itinerant nature of U 5f electrons in UN. The dual nature of 5f electrons was not observed in the present experiment, and an itinerant description is the most realistic starting point to describe the electronic structure of UN. This suggests that the magnetic ordering in UN originates from itinerant U 5f electrons. The magnitude of the magnetic moment in the band-structure calculation in the AFM phase is 0.50 μ_B, while the experimental value is 0.75 μ_B. They are similar in magnitude, and this also supports an itinerant description of U 5f states in UN. Here, it should be noted that the magnetic susceptibility in the PM phase follows the modified Curie-Weiss law above T_N, with an effective moment of 2.65 μ_B.[4] Therefore, the Curie-Weiss behavior in the PM phase also originates from itinerant U 5f electrons. Meanwhile, the changes in ARPES spectra due to the AFM transition were very small. In addition, the Fermi surface of UN has a highly three-dimensional shape, and its nesting region is very small, suggesting that the nesting of Fermi surfaces is unlikely as the origin of the AFM transition. Therefore, although the itinerant description is appropriate for U 5f states, a simple nesting scenario cannot be applied to the AFM ordering in UN. This aspect is consistent with the picture of a weak itinerant antiferromagnetism,[5] where the formation of a gap at E_F is not the main origin of the magnetism.

Here, we consider the changes in ARPES spectra associated with the AFM transition. The changes in spectral function due to the AFM transition have been studied for some itinerant antiferromagnets experimentally.[26–29] The most extensively studied material is chromium metal, which is an itinerant antiferromagnet showing incommensurate spin-density-wave-type ordering. In ARPES studies of chromium metal, the AFM transition was observed in the ARPES spectra as the emergence of back-folded replica bands due to the magnetic Brillouin zone and the formation of a hybridization gap in a large portion of the Fermi surfaces. The back-folded bands are hybridized with the original bands at the boundary of the magnetic Brillouin zone, and the intensity is transferred from

the original bands to the back-folded bands in the vicinity of their crossing points. The spectral intensities of the upper and lower split bands are given by the coherent factors u_p^2 and v_p^2, respectively.[30,31] For UN, the formation of the hybridization gap and the back-folded bands are not as clear as for chromium metal at the zone boundary of the magnetic Brillouin zone. Meanwhile, the position of the band is shifted toward lower binding energies by about 47 meV at the boundary of the magnetic Brillouin zone in which the magnetic moment is directed along the [010] direction as shown in Fig. 3(e). This might be due to the formation of a small hybridization gap in the vicinity of their crossing point. The small gap results from the small hybridization, and the folded bands should have a weak intensity in this case. Therefore, observation of the hybridization gap itself was impossible in the present experiment, but the observed changes might be due to the formation of the gap. The small changes in electronic structure due to the AFM transition are consistent with the picture of a weak itinerant antiferromagnetism where spin-polarized itinerant electrons form moments in both the PM and the AFM phases.

IV. CONCLUSION

In conclusion, we have revealed the band structure and Fermi surfaces of UN by soft x-ray ARPES. Bands with a large contribution from U 5f states formed clearly in the vicinity of E_F, and the dual nature of U 5f electrons was not observed. Both the band structure and the Fermi surfaces in the PM phase were qualitatively explained by the band-structure calculation based on the LDA, which treats all U 5f electrons as being itinerant. The dual nature of U 5f electrons was not observed in the present experiment, and the LDA is a realistic starting point to describe the electronic structure of UN. Meanwhile, the changes in ARPES spectra associated with the AFM transition were very small. The Fermi surfaces of UN have highly three-dimensional structures, suggesting that the nestings of Fermi surfaces are unlikely to be the origin of the AFM ordering.

ACKNOWLEDGMENTS

We thank H. Kusunose of Ehime University and K. Shimada of Hiroshima University for helpful discussions. The experiment was performed under Proposal No. 2006B3808 at SPring-8 BL23SU. The present work was financially supported by a Grant-in-Aid for Scientific Research from the Ministry of Education, Culture, Sports, Science, and Technology, Japan, under Contact No. 21740271, a Grant-in-Aid for Scientific Research on Innovative Areas "Heavy Electrons" (No. 20102003) from the Ministry of Education, Culture, Sports, Science, and Technology, Japan, and Shorei Kenkyuu Funds from the Hyogo Science and Technology Association.

APPENDIX: SIMULATION OF ARPES SPECTRA BASED ON BAND-STRUCTURE CALCULATIONS

In the present study, we have simulated ARPES spectra based on the results of band-structure calculations. Figure 5

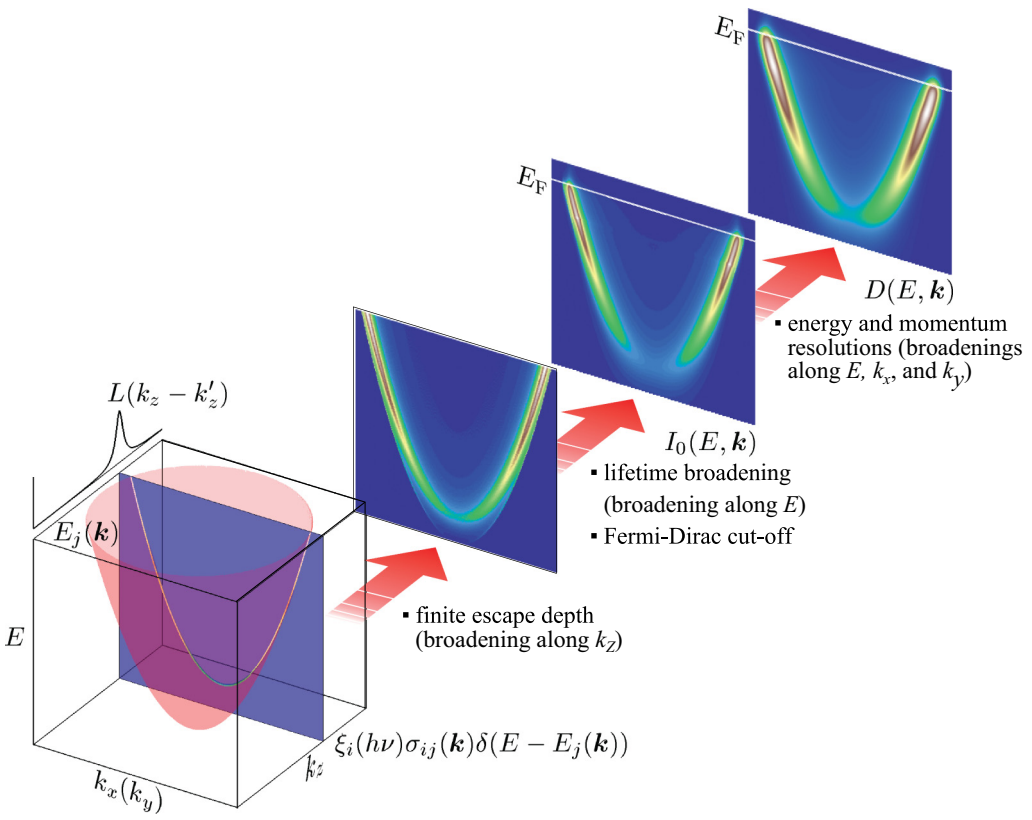

FIG. 5. (Color online) Simulation of ARPES spectra based on band-structure calculation.

shows the procedure for the simulation. First, we take into account the intrinsic effects of the photoemission process such as the damping of the final-state wave functions and the finite lifetime of the photohole.[32] These effects appear as a finite broadening of photoemission spectra along the momentum perpendicular to the surface direction (δk_z) and energy direction (δE), respectively. The matrix-element effect is approximately taken into account by multiplying the calculated photoionization cross section of the atomic orbital $\xi_i(h\nu)$[15] and the orbital character of each eigenvalue in the band-structure calculation $\sigma_{ij}(\boldsymbol{k})$, where i and j represent indices of the orbital and band, respectively. Based on these assumptions, the photoelectron current $I(E,\boldsymbol{k})$ is proportional to $I_0(E,\boldsymbol{k})$ expressed as

$$\begin{aligned} I(E,\boldsymbol{k}) &\propto I_0(E,\boldsymbol{k}) \\ &= f(E)\sum_i\sum_j\int_{-\infty}^{\infty} dk_z'\xi_i(h\nu)\sigma_{ij}(\boldsymbol{k}) \\ &\quad\times\frac{\delta k_z}{(k_z-k_z')^2+(\delta k_z/2)^2}\frac{\delta E}{(E-E_j(\boldsymbol{k}))^2+(\delta E/2)^2}, \end{aligned} \tag{A1}$$

where $E_j(\boldsymbol{k})$ is the energy dispersion of the jth band. This equation corresponds to Eq. (3) in Ref. 33, where we have further taken into account the contribution from the Fermi-Dirac function and assumed that final-state surface transmission $|T^f|$ is constant. Then we take into account extrinsic effects such as the instrumental energy resolution (ΔE) and momentum resolutions along the direction parallel to the sample surface (Δk_x and Δk_y). The photoelectron current is proportional to $D(E,\boldsymbol{k})$ defined as

$$\begin{aligned} D(E,\boldsymbol{k}) &= \int_{-\infty}^{\infty} dE'G(E-E')\Big|_{\Delta=\Delta E} \\ &\quad\times\int_{-\infty}^{\infty} dk_x'G(k_x-k_x')\Big|_{\Delta=\Delta k_x} \\ &\quad\times\int_{-\infty}^{\infty} dk_y'G(k_y-k_y')\Big|_{\Delta=\Delta k_y} I_0(E,\boldsymbol{k}). \end{aligned} \tag{A2}$$

The Gaussian broadening function $G_\Delta(x)$ is expressed as

$$G(x) = \frac{1}{\Delta}\sqrt{\frac{\ln 2}{\pi}}\exp\left\{-\frac{x^2}{(\Delta/2)^2}\right\}, \tag{A3}$$

where $\Delta/2\sqrt{\ln 2}$ is the FWHM. In the present study, the contributions from the U 5f, N 2s, and N 2p states are taken into account since ionization cross sections of the other orbitals are much smaller than the values of these orbitals. The ratio of photoionization cross sections is taken as ξ_{U5f}:ξ_{N2s}:ξ_{N2p} = 1:0.2:0.04 based on the calculated cross sections of atomic orbitals.[15] The broadening along the k_z direction is assumed to be 0.1 Å^{-1}, which corresponds to the escape depth of photoelectrons $\lambda = 10$ Å. Lifetime broadening δE is proportional to $(E-E_F)^2$ near E_F (of the order of a few tens to a few hundred meV) for interacting Fermion systems[34] at absolute zero temperature, but its behavior far below E_F (of the order of several eV) is not well understood. Thus, we have assumed that it has a linear dependence on $(E-E_F)$ on a wide energy scale as has been observed in Ni metal.[35] We have assumed that it is 0 at E_F and 0.5 eV at $E_B = 5$ eV.

*fujimori@spring8.or.jp
†Present address: Japan Synchrotron Radiation Research Institute/SPring-8, Sayo, Hyogo 679-5198, Japan.

[1] T. Durakiewicz, C. D. Batista, J. D. Thompson, C. G. Olson, J. J. Joyce, J. E. Gubernatis, E. Guziewicz, M. T. Butterfield, A. J. Arko, J. Bonća, K. Matternberger, and O. Vogt, Phys. Rev. Lett. **93**, 267205 (2004).
[2] H. Yamagami, T. Ohkochi, S. Fujimori, T. Toshimitsu, A. Yasui, T. Okane, Y. Saitoh, A. Fujimori, Y. Haga, E. Yamamoto, S. Ikeda, and Y. Onuki, J. Phys.: Conf. Ser. **200**, 012229 (2010).
[3] J. M. Fournier, J. Beille, A. Boeuf, C. Vettier, and A. Wedgwood, Physica B **102**, 282 (1980).
[4] M. Samsel-Czekała, E. Talik, P. de V. Du Plessis, R. Troć, H. Misiorek, and C. Sułkowski, Phys. Rev. B **76**, 144426 (2007).
[5] A. Solontsov and V. P. Silin, Phys. Lett. A **334**, 453 (2005).
[6] B. Reihl, G. Hollinger, and F. J. Himpsel, Phys. Rev. B **28**, 1490 (1983).
[7] T. Itoh, H. Kumigashira, S. Souma, T. Takahashi, and T. Suzuki, J. Mag. Mag. Mater. **226–230**, 68 (2001).
[8] L. Black, F. Miserque, T. Gouder, L. Havela, J. Rebizant, and F. Wastin, J. Alloys Compd. **315**, 36 (2001).
[9] T. M. Holden, W. J. L. Buyers, E. C. Svensson, and G. H. Lander, Phys. Rev. B **30**, 114 (1984).
[10] P. Modak and A. K. Verma, Phys. Rev. B **84**, 024108 (2011).
[11] Q. Y. Yin, A. Kutepov, K. Haule, G. Kotliar, S. Y. Savrasov, and W. E. Pickett, Phys. Rev. B **84**, 195111 (2011).
[12] T. Abram and S. Ion, Energy Policy **36**, 4323 (2008).
[13] Yu. F. Zhukovskii, D. Bocharov, E. A. Kotomin, R. A. Evarestov, and A. V. Bandura, Surf. Sci. **603**, 50 (2009).
[14] A. Yokoya, T. Sekiguchi, Y. Saitoh, T. Okane, T. Nakatani, T. Shimada, H. Kobayashi, M. Takao, Y. Teraoka, Y. Hayashi, S. Sasaki, Y. Miyahara, T. Harami, and T. A. Sasaki, J. Synchrotron Rad. **5**, 10 (1998).
[15] J. J. Yeh and I. Lindau, At. Data Nucl. Data Tables **32**, 1 (1985).
[16] H. Yamagami, J. Phys. Soc. Jpn. **67**, 3176 (1998).
[17] U. von Barth and L. Hedin, J. Phys. C **5**, 1629 (1972).
[18] S. Fujimori, T. Ohkochi, I. Kawasaki, A. Yasui, Y. Takeda, T. Okane, Y. Saitoh, A. Fujimori, H. Yamagami, Y. Haga, E. Yamamoto, Y. Tokiwa, S. Ikeda, T. Sugai, H. Ohkuni, N. Kimura, and Y. Ōnuki, J. Phys. Soc. Jpn. **81**, 014703 (2012).
[19] L. Havela, F. Wastin, J. Rebizant, and T. Gouder, Phys. Rev. B **68**, 085101 (2003).
[20] T. Ohkochi, S. I. Fujimori, H. Yamagami, T. Okane, Y. Saitoh, A. Fujimori, Y. Haga, E. Yamamoto, and Y. Ōnuki, Phys. Rev. B **78**, 165110 (2008).
[21] H. Daimon, S. Imada, H. Nishimoto, and S. Suga, J. Electron Spectrosc. Relat. Phenom. **76**, 487 (1995).
[22] R. Atta-Fynn and A. K. Ray, Phys. Rev. B **76**, 115101 (2007).

[23]L. Petit, A. Svane, Z. Szotek, W. M. Temmerman, and G. M. Stocks, Phys. Rev. B **80**, 045124 (2009).
[24]X. Yang, P. S. Riseborough, C. G. Olson, J. J. Joyce, E. D. Bauer, J. L. Sarrao, D. P. Moore, K. S. Graha, S. Elgazzar, P. M. Oppeneer, E. Guziewicz, and M. T. Butterfield, Philos. Mag. **89**, 1893 (2009).
[25]X. Y. Cui, K. Shimada, Y. Sakisaka, H. Kato, M. Hoesch, T. Oguchi, Y. Aiura, H. Namatame, and M. Taniguchi, Phys. Rev. B **82**, 195132 (2010).
[26]J. Shäfer, E. Rotenberg, S. D. Kevan, and P. Blaha, Surf. Sci. **454–456**, 885 (2000).
[27]E. Rotenberg, B. K. Freelon, H. Koh, A. Bostwick, K. Rossnagel, A. Schmid, and S. D. Kevan, New J. Phys. **7**, 114 (2005).
[28]E. Rotenberg, O. Krupin, and S. D. Kevan, New J. Phys. **10**, 023003 (2008).
[29]M. Yi, D. H. Lu, J. G. Analytis, J.-H. Chu, S.-K. Mo, R.-H. He, M. Hashimoto, R. G. Moore, I. I. Mazin, D. J. Singh, Z. Hussain, I. R. Fisher, and Z.-X. Shen, Phys. Rev. B **80**, 174510 (2009).
[30]A. P. Kampf and J. R. Schrieffer, Phys. Rev. B **42**, 7967 (1990).
[31]J. R. Schrieffer and A. P. Kampf, J. Phys. Chem. Solid **56**, 1673 (1995).
[32]H. Wadati, T. Yoshida, A. Chikamatsu, H. Kumigashira, M. Oshima, H. Eisaki, Z.-X. Shen, T. Mizokawa, and A. Fujimori, Phase Trans. **79**, 617 (2006).
[33]V. N. Strocov, J. Electron Spectrosc. Relat. Phenom. **130**, 65 (2003).
[34]J. M. Luttinger, Phys. Rev. **121**, 942 (1961).
[35]W. Eberhardt and E. W. Plummer, Phys. Rev. B **21**, 3245 (1980).